MADRID
inter.noise 2019
June 16 - 19
NOISE CONTROL FOR A BETTER ENVIRONMENT

Test methodologies for mapping tyre exterior noise in semi-anechoic chamber

Corradi, Roberto[1]
Department of Mechanical Engineering, Politecnico di Milano
Via La Masa 1, Milano, Italy

Ripamonti, Francesco[2]
Department of Mechanical Engineering, Politecnico di Milano
Via La Masa 1, Milano, Italy

Di Lione, Riccardo
Pirelli Tyre SpA
Viale Piero e Alberto Pirelli 25, Milano, Italy

Caccialanza, Matteo
Pirelli Tyre SpA
Viale Piero e Alberto Pirelli 25, Milano, Italy

ABSTRACT

Tyre exterior noise is the result of the combination of many complex phenomena taking place at tyre/road contact. Tread impact, stick/slip of the tread blocks and air-pumping are only some of the excitation mechanisms, whose effect can be amplified by the tyre structural vibrations, by the pipe resonances of the longitudinal grooves in the contact patch and by the aerodynamic phenomena in the leading and trailing footprint regions. Indoor tests are of fundamental support in the development of new products, in terms of optimization of both tread pattern design and structural solutions. This paper illustrates the test methodologies developed within a research cooperation between Politecnico di Milano and Pirelli Tyre, for mapping the noise generated by a rolling tyre during the experiments carried out in semi-anechoic chamber. Noise source identification is performed through microphone array techniques, while the radiated sound field is characterized in terms of directivity patterns for variable frequency. In both cases the measurement equipment is fitted with a robotic handling system to speed up the stepped positioning of the microphones.

Keywords: Noise source mapping, sound field maps, Tyre noise
I-INCE Classification of Subject Number: 72

[1] Roberto.corradi@polimi.it
[2] Francesco.ripamonti@polimi.it

1. INTRODUCTION

The progressive reduction of vehicle exterior noise generated by the engine and other sources (such as intake&exhaust systems or gearbox) exalts the importance of the tyre rolling noise contribution. Starting from the 70s, a huge number of research activities focused on this topic. As stated in [10], tyre noise is the result of the combination of many complex phenomena: tread impact, stick/slip of the tread blocks and air-pumping in/out of the cavities within the tyre footprint are only some of the excitation mechanisms, whose effect can be amplified by the tyre structural vibrations, by the pipe resonances in the channels formed by the tread pattern in the contact patch and by the aerodynamic phenomena in the leading and trailing footprint regions [10]. A full understanding of the quantitative importance of the different phenomena has not yet been reached and the influence of tyre design parameters on tyre/road noise generation still needs to be clarified.

In this context, the present work aims at investigating different experimental methodologies for mapping tyre exterior noise and for supporting product development. Two commercial tyres, mounted on a test vehicle, have been studied in an indoor environment, the semi-anechoic chamber of the Pirelli R&D centre in Milan, Italy. In order to achieve a global characterization of the acoustic behaviour of the tyre, two methodologies have been employed during the experimental tests: acoustic mapping techniques based on microphone arrays (Beamforming and Planar Nearfield Acoustic Holography [3][4][5][6][8]) and sound directivity measurements, inspired to the ISO 3744 Standard [9]. The influence of the vehicle speed has been studied by repeating the tests at 50, 80 and 110 km/h, although in this paper only the 80 km/h results are presented and discussed.

2. EXPERIMENTAL SETUP

Figure 1. The semi-anechoic chamber at the Pirelli R&D headquarter in Milan

The experimental campaign was carried out in the semi-anechoic chamber of Pirelli R&D headquarter in Milan, Italy (Figure 1). The test room, whose dimensions are 10m x 7m x 5m, is equipped with a rolling drum that allows one of the wheels to be put in rotation. The drum surface is characterized by a controlled roughness.

During the tests, the vehicle (a VW GOLF-MKVI) was equipped with two different commercial tyres (namely tyre A and B), characterized by very similar noise

levels. This choice allows verifying the effectiveness of the adopted methodologies in pointing out the small differences between the two samples. As previously introduced, the tests are performed at the reference speed of 80 km/h, with the testing tyre mounted in front-right position.
The experimental set-up is composed by a laser tacho probe, placed under the car body and used for measuring the angular speed of the rolling tyre and also for synchronizing the recorded signals. As for the sound pressure measurements, at the base of the proposed methodologies, free-field PCB microphones (1/2", 32 mV/Pa, frequency range 20-20000 Hz) have been adopted.
Based on the knowledge of the generation mechanisms and amplification phenomena of the tyre noise, the analysis has been limited to the range 160-5000 Hz, setting the sampling frequency to 12500 Hz and the reference duration of the acquired time histories to 5 seconds. However, results are presented in the range 630-2000 Hz, since this paper is focused on the most relevant contributions associated to the tread pattern harmonics and the pipe resonance [12]. Indeed, at lower frequencies only one contribution (at about 200-250 Hz) is present, probably related to the tyre cavity noise [14][15] and not particularly interesting for the study of the exterior noise. On the other side, at higher frequencies the sound pressure levels are significantly reduced (approximatively 10-15 dB less).

3. NOISE SOURCE IDENTIFICATION

3.1 Test methodology

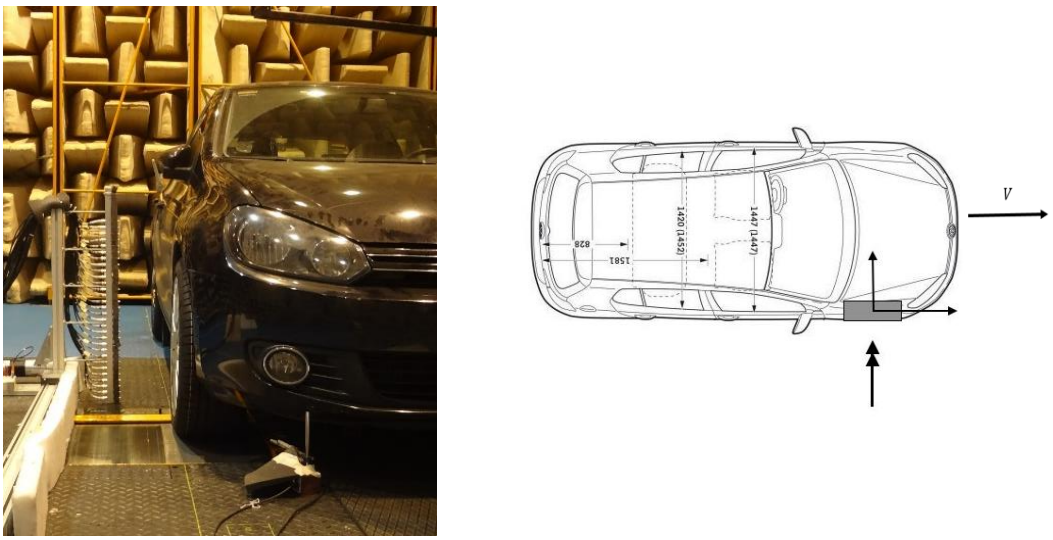

Figure 2. The experimental setup for noise source mapping through the microphone array

In this work two noise source mapping techniques (the Beamforming and the Planar Nearfield Acoustic Holography) have been applied (Figure *2*).

A vertical array of 31 microphones with a regular spacing of 25 mm is mounted on a robotic slider. Its position is controlled from remote and, based on the stationarity of the phenomenon, a stepped acquisition is carried out (25 mm lateral steps). At the end of the scan a total of 1271 measuring points are covered, corresponding to an equivalent planar array with dimensions 1 m width per 0.75 m height. The acquired data are then

synchronized thanks to the trigger signal of the tacho probe through an order tracking procedure [13] and they are finally ready for source mapping post-processing.

Planar Nearfield Acoustic Holography (PNAH)

The PNAH is an experimental technique that, starting from the sound pressure measurements on a planar grid, is able to provide a three-dimensional reconstruction of the acoustic field, considering planes parallel to the one used for measurements [11][12]. The time domain signals over the 2D grid are firstly translated in the frequency domain and then in wave numbers domain, through a 2D Fourier Spatial Transformation. The information is propagated on the target plane and finally it is possible to come back to the time domain applying the inverse transformations. Working in the nearfield region, the method processes the evanescent waves, preserving good performances in terms of spatial resolution also at the low frequencies. The PNAH spatial resolution can be calculated as

$$SR_{PNAH} = \frac{1}{2\Delta} \tag{1}$$

where Δ is the distance between two adjacent measuring points (25 mm in our case). On the other side, a drawback of this technique is related to the fact that from the mathematical point of view it represents an ill-posed inverse problem and numerical instabilities due to the backward propagation of small perturbations in the original measurements can occur. To contrast this issue, the holography regulation procedure adopts the Harris filter, whose parameters are tuned through a trial and error approach [3][4].

Delay&Sum Beamforming (BF)

Besides PNAH, a second well-known technique (the BF) has been applied to the data acquired by the microphone array. Basically, the method scans a grid of nodes on a generic surface, assuming that each node, or location, represents a potential sound source [1][2][5]. Applying the Delay&Sum algorithm, the sound pressure at each location s_{loc} is estimated by averaging the microphone signals s_i, phased at the emission time and amplified by the acoustic path

$$S_{loc}(t) = \frac{1}{N}\sum_1^N s_i\left(t + \frac{R_{i,loc}}{c}\right) R_{i,loc} \tag{2}$$

The maximum output amplitude is achieved when the phased signals are coherent each other, i.e. when the location corresponds to a sound source.
For the BF, the spatial resolution can be estimated through the Rayleigh formula

$$SR_{BF} = \frac{L}{y_m c} f \tag{3}$$

It is proportional to the ratio between the overall size of the array L and the microphone-to-source distance y_m and, unlike the PNAH, it linearly increases with the frequency under investigation f (improving its performances) [7][8].

The correct choice between the two post-processing methods allows to get the best spatial resolution with respect to the analysed frequency band. In this application, considering the array dimensions and the distance between the tyre and the microphones plane (200 mm), below a threshold frequency of 1.3 kHz the PNAH has a higher

resolution, while above this limit the BF is better and its resolution gradually increases. The upper limit to avoid spatial aliasing with this array is set to 13.72 kHz [7][8].

3.2 Results

In Figure 3 the results of noise source identification for the two tested tyres are shown, for three following 1/3 octave band central frequencies: 800 Hz, 1000 Hz (with PNAH) and 2000 Hz (with BF).
It is possible to notice that the sound sources are always located close to the contact patch area, showing two predominant contributions at the leading and the trailing edges. Considering the same frequency band, the behaviour of the two tyres is similar. However, at mid-low frequencies tyre B presents higher levels at the leading edge, while sound radiation is more symmetric for tyre A. At higher frequency the trailing edge region dominates on both tyres in terms of extension and intensity.

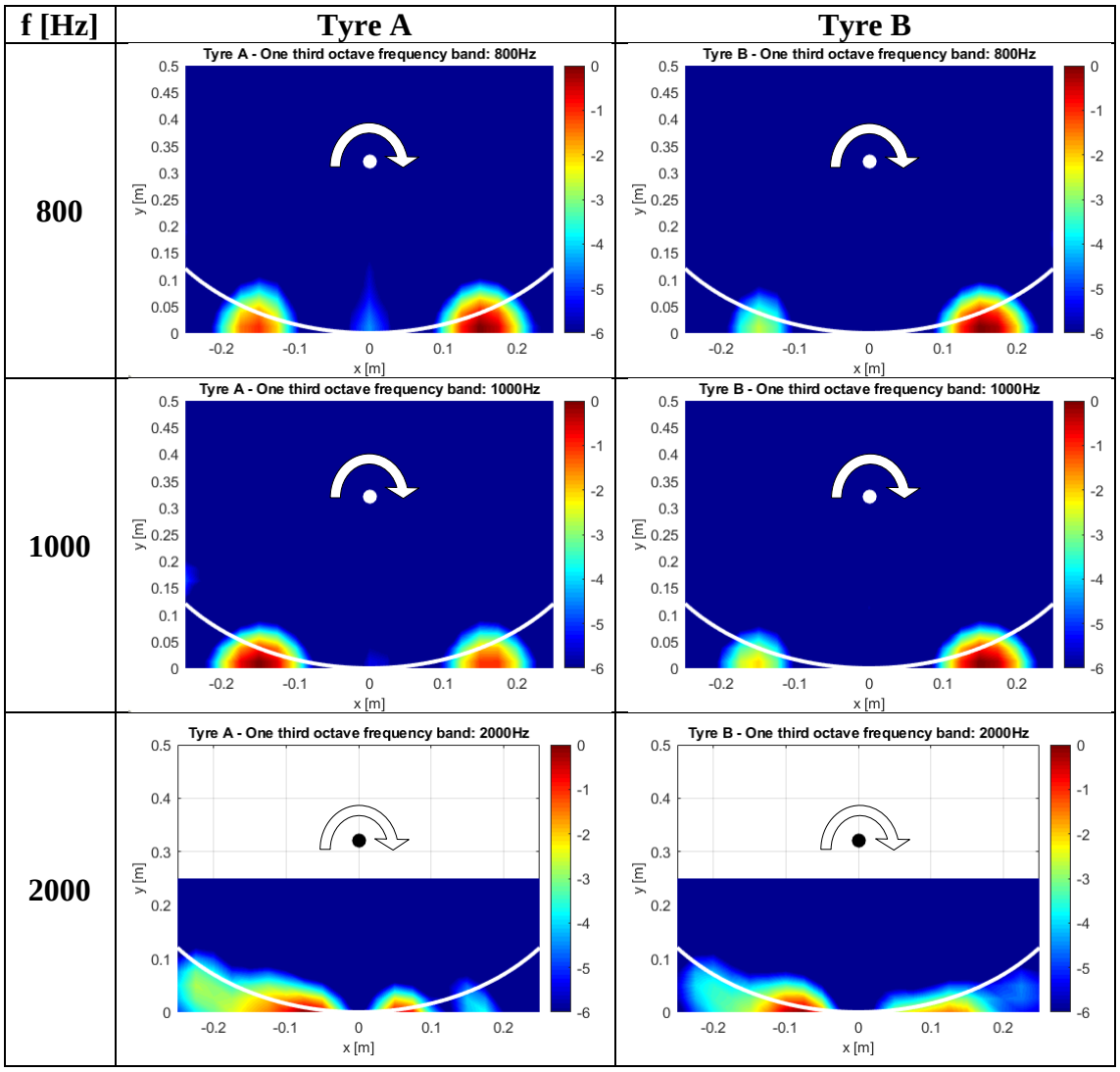

Figure 3. Noise source maps for tyre A and tyre B corresponding to three frequency bands

4. SOUND FIELD MAPPING

4.1 Test methodology

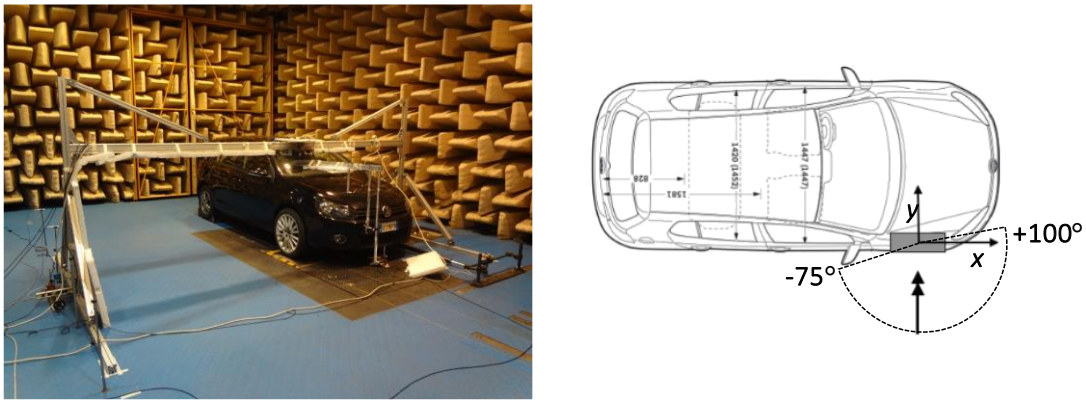

Figure 4. The experimental setup for sound field mapping

The methodologies presented so far allow identifying the noise sources located at the footprint region. However, in order to collect comprehensive data useful for interpreting the phenomena associated to tyre noise generation and for supporting the product development, the acoustic field has also been mapped. An experimental set-up inspired to the ISO 3744 standard [9] has been developed to perform sound directivity measurements. Figure 4 shows the measuring system made of four PCB microphones mounted on an arc-shaped rigid arm rotating about a vertical axis centred in the tyre contact patch. The frame is moved by a turning table positioned at the top of a supporting structure and the microphones move over a quarter spherical surface surrounding the tyre, delimited horizontally by the chamber floor and vertically by the car body side.

The radius of the sphere is 1.2 m and for frequencies above 300 Hz it is sufficiently large to satisfy the assumption of far-field, as required for the directivity pattern evaluation. The angular positions range between -75 and +100 deg (angle 0 deg corresponding to the direction of the tyre rotation axis).

For each microphone 37 discrete measurement positions can be analysed, located on a circumference with a step of 5 deg. The results shown hereafter refer only to microphone 4 (at the height of 180 mm from the chamber floor), that is aligned with respect to a propagation direction representative of a receiver positioned on the roadside. Then data are processed in the frequency domain and the sound pressure RMS are computed for the generic narrow or 1/3 octave band.

The directivity factor Q is calculated as

$$\bar{I} = \frac{1}{n}\sum_1^n I(\vartheta_n) \quad \rightarrow \quad Q(\vartheta_n) = \frac{I(\vartheta_n)}{\bar{I}} \tag{4}$$

where n is the number of measurement positions (37) and ϑ_n the measuring direction in the range [-75 100] deg. Under the far-field assumption the sound intensity I for each angle can be calculated as

$$I = \frac{p_{rms}^2}{\rho_0 c} \tag{5}$$

where p_{rms} is the sound pressure RMS, ρ_0 is the air density and c is the sound speed in air, in standard conditions (environmental pressure and temperature respectively equal to 1 bar and 20C). Finally, the directivity factor Q is reported in terms of Directivity Index

$$DI(\vartheta) = 10\log(Q_i(\vartheta)) \quad (6)$$

4.2 Results

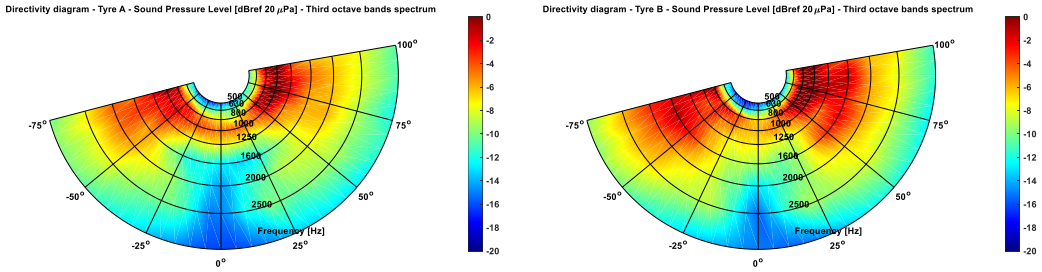

Figure 5. The sound field maps for tyre A and B as a function of frequency and angular position

Figure 5 shows the sound field maps of tyre A and B as a function of frequency and angular position. Results are normalized with respect to the maximum RMS value and reported in terms of sound pressure level (Lp).

At frequencies associated to generation mechanisms and amplification phenomena such as the 1st tread pattern harmonics and the pipe resonance (800-1000 Hz), dark red spots in the trailing and especially in the leading-edge regions are evident for both tyres. For tyre B, the high Lp at the leading edge extends up to 2 kHz. These results confirm what already observed analysing the noise source maps (see Figure 3).

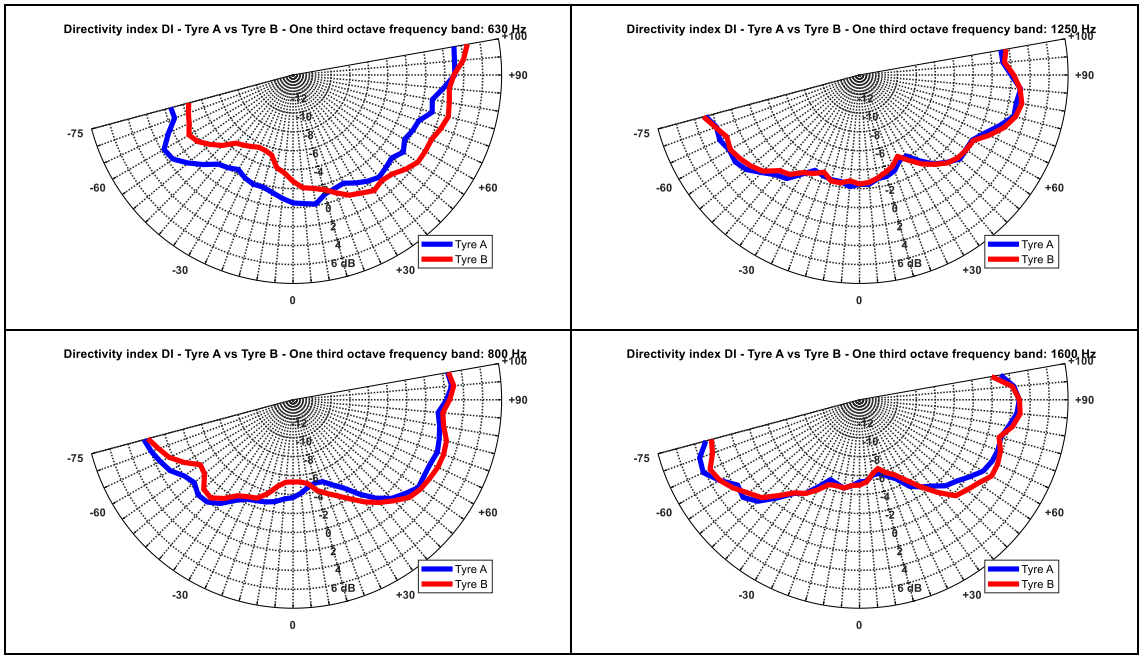

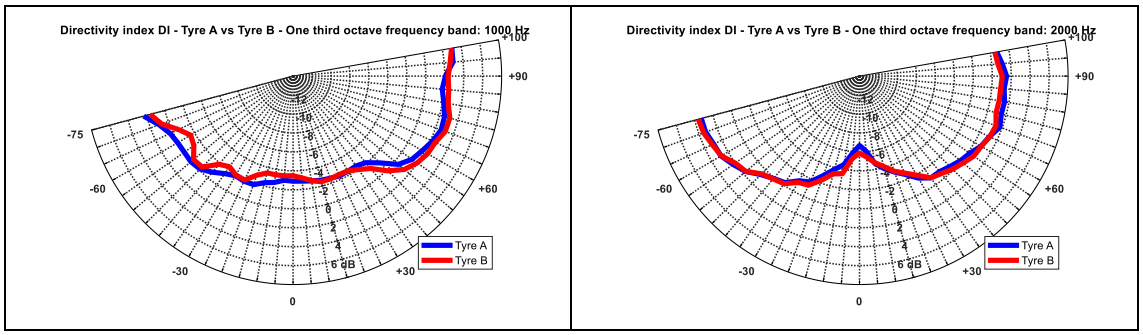

Figure 6. The comparison between the directivity patterns of tyres A and B for different frequency bands

In Figure 6 a comparison between the directivity patterns of the two tyres is reported for different 1/3 octave bands in the range 630-2000 Hz. The diagrams demonstrate that the directivity is very similar (excluding the lowest frequency) and the stretched shapes confirm again that the most emitting regions are located at the leading and trailing edge.

However, in order to complete the comparison between tyre A and tyre B, the differences between the average sound intensity levels ($L_{I,B}$- $L_{I,A}$) for six following 1/3 octave bands are summarized in Table 1. Tyre A behaves better that B in almost all the considered bands, except at 1 kHz where tyre B is more silent because it is probably less sensitive to the pipe resonance amplification.

Table 1. Difference in the average sound intensity ($L_{I,B}$- $L_{I,A}$) for different frequency bands

Frequency [Hz]	**630**	**800**	**1000**	**1250**	**1600**	**2000**
Lp (B-A) [dB]	+0.2	+2.9	-1.0	+0.3	+3.7	+1.0

5. CONCLUSIONS

This paper presented different indoor experimental methodologies for mapping tyre exterior noise and for supporting product development. During the tests two commercial tyres have been compared in the Pirelli R&D semi-anechoic chamber.

Two noise source mapping techniques (the Beamforming and the Planar Nearfield Acoustic Holography) have been applied, allowing to identify predominant contributions located at the leading and the trailing edges. In order to collect comprehensive data useful for interpreting the phenomena associated to tyre noise generation, the acoustic field has also been mapped by means of sound pattern measurements. A good correlation between the results coming from the different employed techniques has been observed.

ACKNOWLEDGEMENTS

The authors gratefully acknowledge Pirelli Tyre Team (Eng. Fioravanti and Sabato) for providing the support and materials necessary for this work.

REFERENCES

[1] J. Billingsley, R. Kinns, The acoustic telescope, Journal of Sound and Vibration 48 (October 22) (1976) 485–510.

[2] M. Mosher, M.E. Watts, Calibration of microphone arrays for phased array processing, AIAA 97-1678.
[3] E.G. Williams, Fourier Acoustics-Sound Radiation and Nearfield Acoustical Holography, Academic Press, New York, 1999.
[4] J.D. Maynard, E.G. Williams, Y. Lee, Nearfield acoustic holography: I, Theory of generalized holography and the development of NAH, Journal of Acoustical Society of America 78 (4) (1985) 1395–1413.
[5] Don H. Johnson, Dan E. Dudgeon, Array Signal Processing: Concepts and Techniques, Prentice Hall Signal Processing Series, 1993.
[6] W.M. Humphreys Jr., T.F. Brooks, W.W. Hunter Jr., K.R. Meadows, Design and use of microphones directional arrays for aeroacoustic measurements, AIAA 98-0471, 1998.
[7] Cigada, A., Lurati, M., Ripamonti, F., Vanali, M. Moving microphone arrays to reduce spatial aliasing in the beamforming technique: Theoretical background and numerical investigation (2009) Journal of the Acoustical Society of America, 124 (6), pp. 3648-3658.
[8] Cigada, A., Ripamonti, F., Vanali, M. The delay & sum algorithm applied to microphone array measurements: Numerical analysis and experimental validation (2007) Mechanical Systems and Signal Processing, 21 (6), pp. 2645-2664.
[9] UNI EN ISO 3744:2010. “Acoustics - Determination of sound power levels and sound energy levels of noise sources using sound pressure - Engineering methods for an essentially free field over a reflecting plane”.
[10] Sandberg, U. and Ejsmont, J.A. Tyre/road Noise Reference Book, 2002, Informex.
[11] Pasha, H. G. Lens-less Photography of Sound - Near-field Acoustic Holography (2007).
[12] J.S. Bolton, H.S. Kwon, Nearfield acoustical holography applied to sound radiation from tires, Purdue University, Indiana, (1998).
[13] K.R. Fyfe, E.D.S. Munck, ANALYSIS OF COMPUTED ORDER TRACKING, Mechanical Systems and Signal Processing, Volume 11, Issue 2, (1997), Pages 187-205.
[14] T. Sakata, H. Morimura, H. Ide, Effects of tyre cavity resonance on vehicle road noise, Tyre Science and Technology 18 (1990) 68-79.
[15] J. Thompson, Plane wave 1 resonance in the air cavity as a vehicle interior noise source, Tyre Science and Technology 23 (1995) 2-10.